Image denoising in bidimensional empirical mode decomposition domain: the role of Student's probability distribution function

Salim Lahmiri ✉

Department of Electrical Engineering, École de Technologie Supréireure, Montreal, Canada
✉ *E-mail: Salim.lahmiri.1@ens.etsmtl.ca*

Published in Healthcare Technology Letters; Received on 18th March 2015; Revised on 31st July 2015; Accepted on 21st August 2015

Hybridisation of the bi-dimensional empirical mode decomposition (BEMD) with denoising techniques has been proposed in the literature as an effective approach for image denoising. In this Letter, the Student's probability density function is introduced in the computation of the mean envelope of the data during the BEMD sifting process to make it robust to values that are far from the mean. The resulting BEMD is denoted tBEMD. In order to show the effectiveness of the tBEMD, several image denoising techniques in tBEMD domain are employed; namely, fourth order partial differential equation (PDE), linear complex diffusion process (LCDP), non-linear complex diffusion process (NLCDP), and the discrete wavelet transform (DWT). Two biomedical images and a standard digital image were considered for experiments. The original images were corrupted with additive Gaussian noise with three different levels. Based on peak-signal-to-noise ratio, the experimental results show that PDE, LCDP, NLCDP, and DWT all perform better in the tBEMD than in the classical BEMD domain. It is also found that tBEMD is faster than classical BEMD when the noise level is low. When it is high, the computational cost in terms of processing time is similar. The effectiveness of the presented approach makes it promising for clinical applications.

1. Introduction: The bi-dimensional empirical mode decomposition (BEMD) is the two-dimensional (2D) version of the original empirical mode decomposition of Huang *et al.* [1] which is an adaptive multi-resolution analysis technique that decomposes a given signal into a finite sum of components called intrinsic mode functions (IMFs), plus a residue. The empirical mode decomposition algorithm is based on a sifting process that successively estimates the mean envelope of an unknown signal as the average of the upper and lower envelopes, minus a residual component. In particular, low order IMFs represent fast oscillations (high frequency modes), and high order IMFs represent slow oscillations (low frequency modes). The IMFs are local and auto-adaptive to the input data. Hence, the merit of using the EMD is that it is driven by the input data. Unlike the wavelet transform, the EMD does not require a-priori basis function selection, since the IMFs are automatically derived from the input signal. In addition, the EMD is effective for the analysis of both stationary and non-stationary signals, and it is a non-linear decomposition technique.

To address the problem of mean sensibility to outliers during the sifting process, an adjusted empirical mode decomposition method built on Student's probability density function (PDF) denoted by tEMD [2] where the data was transformed with the Student PDF prior to computation. Because Student's PDF has longer tails than the normal distribution, it is more robust to values that are far from the mean. In particular, it is less susceptible to signal variance fluctuations, which may lead to more representative mean envelope curves when applying the EMD algorithm. The tEMD was found to be more effective than the traditional EMD in modelling a simulated signal, an electrocardiogram (ECG) record, and the S&P500 closing prices [2].

Following our previous promising results when using EMD for biomedical image classification [3, 4] and ECG denosing [5], and tEMD for physiological signal modelling, we recently extend the one-dimensional tEMD to 2D tEMD for the analysis and classification of pathological retina images [6] by developing a computer aided diagnosis tools for automatic retina pathology grading. Tests comparing the 2D-EMD and 2D-tEMD indicated that the latter outperformed the former for blot hemmorage grading and subretinal exudate grading in digital retinal images.

The purpose of this study is to test the effectiveness of 2D-tEMD against the classical 2D-EMD in image denoising as the latter has gained interest in this area [7–10]. In these previous works, the BEMD was applied to the noisy image to obtain a set of its bi-dimensional intrinsic mode functions (BIMFs). Then, the discrete wavelet transform (DWT) or partial differential equations (PDE) were applied to each of the BIMFs for denoising purpose. Finally, the denoised image is reconstructed based on the denoised BIMFs. Similarly, we apply the DWT [11–13], fourth-order PDE (FOPDE) [14], and linear and non-linear complex diffusion processes (NLCDP) [15] to each extracted tBIMF (BIMFs where Student's PDF is incorporated in mean envelope computation) for denoising purpose. The denoised image is recovered by summing up all the denoised tBIMFs.

The wavelet thresholding technique is commonly used for image denoising given the ability of wavelet analysis to separate noise from the image signal [11–13]. In this study, it is used as the main reference denoising approach against three advanced denoising techniques in BEMD and tBEMD domains; namely the FOPDE and the linear and NLCDP denoted, respectively, linear complex diffusion process (LCDP) and NLCDP. The FOPDE is employed as it avoids blocky effects while achieving good tradeoff between noise removal and edge preservation [14]. The LCDP and NLCDP combine the diffusion equation with the free Schrödinger equation [15]. The main advantages of complex diffusion processes follow [15]. First, there exists a stable diffusion process over the wide range of the angular orientation. Second, the real function behaves like a real linear diffusion process, whereas the imaginary part approximates a smoothed second derivative of the real part, and serves as an edge detector. Third, the complex diffusion enables better performance in different non-linear tasks such as ramp denoising and regularisation of shock filters. In our study, the performance of each denoising approach is evaluated based on the well-known peak-signal-to-noise ratio (PSNR).

The rest of the Letter follows. Section 2 presents the BEMD, tBEMD, PDE, LCDP, NLCDP, and DWT. Section 3 presents the results. Section 4 concludes our study.

2. Methods: As mentioned in introduction, we rely on BEMD and tBEMD to denoise original images corrupted with Gaussian noise.

In particular, classical DWT, FOPDE, and LCDP and NLCDP are employed to denoise each obtained BIMF/tBIMF. The resulting denoised image is obtained by summing up all denoised BIMFs/tBIMFs. In our study, the optimal threshold is determined according to the adaptive threshold selection using principle of Stein's unbiased risk estimate.

2.1. Bi-dimensional empirical mode decomposition: The sifting process of a 2D image $I(x, y)$ is given as follows [10]:

(1) Initialisation: $\text{res}(x, y) = I(x, y)$.
(2) Identify all minima and maxima of $I(x, y)$.
(3) Compute the lower $E_{\text{dw}}(x, y)$ and upper $E_{\text{up}}(x, y)$ envelopes by interpolation of minima and maxima.
(4) Compute the envelope mean as: $M_{\text{en}}(x, y) = (E_{\text{dw}}(x, y) + E_{\text{up}}(x, y))/2$
(5) Subtract $M_{\text{en}}(x, y)$ from $\text{res}(x, y)$ as follows

$$\text{Mod}(x, y) = \text{res}(x, y) - M_{\text{en}}(x, y)$$

(6) If $Mod(x, y)$ is not BIMF, $\text{res}(x, y) = Mod(x, y)$, turn to step 1.
(7) Obtain BIMF: $\text{BIMF}(x, y) = \text{Mod}(x, y)$
(8) $\text{res}(x, y) = \text{res}(x, y) - \text{BIMF}(x, y)$
(9) Repeat steps 1–8 until the residue $\text{res}(x, y)$ satisfies a stopping condition.

Finally, the image $I(x, y)$ can be expressed as follows

$$f(x, y) = \sum_{i=1}^{N} \text{BIMF}_i(x, y) + \text{res}(x, y) \tag{1}$$

where N is the number of BIMFs. In this Letter, the stopping condition is the number of BIMFs set in advance; for instance, three BIMFs plus a residue for simplicity.

In this study, the algorithm to compute the mean envelope is modified to obtain the 2D-tEMD

$$M_{\text{en}}(x, y) = \left(S(E_{\text{dw}}(x, y)) + S(E_{\text{up}}(x, y))\right)/2 \tag{2}$$

where $S(\cdot)$ is the Student PDF. For instance, the Student PDF for a real valued pixel p is given by

$$S(p, \nu) = \frac{1}{\sqrt{(\nu\pi)^d}} \frac{\Gamma((\nu+1)/2)}{\Gamma(\nu/2)} \left(1 + \frac{p^2}{\nu}\right)^{-(\nu+1)/2} \tag{3}$$

where ν is a positive scalar used to capture the distribution tails and $\Gamma(\cdot)$ is the gamma function. In our work, the parameter ν is set to one to better capture heavy tails in the pixels distribution.

The main popular interpolation techniques used to build the upper and the lower envelopes in BEMD are the radial basis function and the triangular interpolation technique. The former generates a smoother surface with high computational cost since all given points are needed to determine a value at any point. In the latter interpolation scheme, a triangular grid for scattered data points is created and a subsequent piecewise interpolation on triangles is used to create an approximated surface. It produces a less smooth surface than radial basis function interpolation technique; but, its computational cost is much lower because it uses only neighbouring points while neglecting all points distant from the centre. The triangular-based linear interpolation is adopted to speed up image decomposition process.

2.2. DWT approach: Wavelet thresholding involves threes steps [11–13]. First, the image is processed with a DWT [15] for decomposition purpose. As a result, the image is decomposed into low-low, low-high, high-low, and high-high sub-band. Then, a non-linear thresholding is performed on each DWT sub-band coefficient. In particular, if the DWT coefficient is smaller than the threshold it is set to zero. Otherwise, it is kept as such or modified. Finally, an inverse DWT is performed to recover the denoised image. In this Letter, the optimal threshold is determined according to the adaptive threshold selection using principle of Stein's unbiased risk estimate [11, 12].

2.3. Fourth-order PDE: For $(x, y) \in \Omega$, let $u(x, y)$ and $u_0(x, y)$ be, respectively, a digital image and its observation with random noise $\varepsilon(x, y)$. The purpose is to find a new image by minimising the cost functional $E(u)$ given by [13]

$$E(u) = \int_{\Omega} f(|\nabla^2 u|)\, \text{d}x\, \text{d}y \tag{4}$$

where ∇^2 is the Laplacian operator and $f(\cdot) \geq 0$ and also $f'(\cdot) > 0$. With the observed image as the initial condition, the solution is given by the following PDE as the time script tends to infinity

$$\frac{\partial u}{\partial t} = -\nabla^2 \left[f'(|\nabla^2 u|) \frac{\nabla^2 u}{|\nabla^2 u|} \right] \tag{5}$$

The minimisation of the functional is equivalent to smoothing the image [14].

2.4. Complex diffusion processes: Consider the initial value problem for a 1D signal

$$\begin{aligned} I_t &= cI_{xx}, \quad t > 0, \quad x, c \in \Re \\ I(x; 0) &= I_0 \in \Re, \end{aligned} \tag{6}$$

where c is a real valued diffusion coefficient. The complex fundamental solution $h(x;t)$ should satisfy the following relationship [15]

$$I(x; t) = I_0 * h(x; t) \tag{7}$$

where * denotes convolution. By rewriting the complex diffusion coefficient as $c = re^{i\theta}$, the fundamental solution is given by [15]

$$h(x; t) = g_\sigma(x; t)\, \text{e}^{i\alpha(x;t)} \tag{8}$$

where $\text{g}(\cdot)$, σ, α, and θ are, respectively, the Gaussian function, its standard deviation, the exponent function, and the angle. They are given by

$$\begin{aligned} \alpha(x; t) &= \frac{x^2 \sin\theta}{4\text{tr}}, \quad \sigma(t) = \sqrt{\frac{2\text{tr}}{\cos\theta}}, \\ g_\sigma(x; t) &= \frac{1}{\sqrt{2\pi\sigma(t)}}\, \text{e}^{-x^2/2\sigma^2(t)} \end{aligned} \tag{9}$$

The NLCDP equation is given by [15]

$$I_t = \frac{\partial}{\partial x}(c(\cdot) I_x), \quad c(s) = c(|I_{xx}|) \tag{10}$$

Then, the general solution is given by

$$I_t = \frac{\partial}{\partial x}\left(\frac{I_x}{1 + I_{xx}^2}\right) = \frac{1 + I_{xx}^2 - 2I_x I_{xxx}}{\left(1 + I_{xx}^2\right)^2} I_{xx} \tag{11}$$

doi: 10.1049/htl.2015.0007

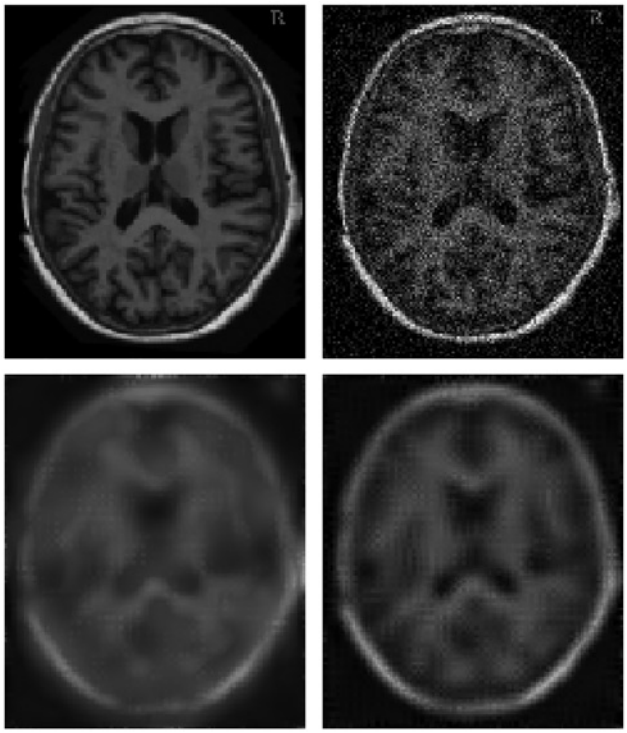

Fig. 1 *Top left-hand side: original brain MRI. Top right-hand side: noisy image with S1. Bottom left-hand side: denoised image based on BEMD-PDE. Bottom right-hand side: denoised image based on tBEMD-PDE*

2.5. Performance measures: The effectiveness of each image denoising approach is measured by the well-known PSNR given by

$$\mathrm{PSNR} = 20\log_{10}\left(\frac{\mathrm{MAX}_f}{\sqrt{\mathrm{MSE}}}\right) \tag{12}$$

where, MAX is the maximum signal value in the original image f of size $m \times n$, and MSE is the mean squared error.

3. Experimental results: The proposed image denoising approaches were applied to two biomedical images and a standard image widely used in image processing: Lena image (225×225), brain MRI (256×256), and prostate tissue image

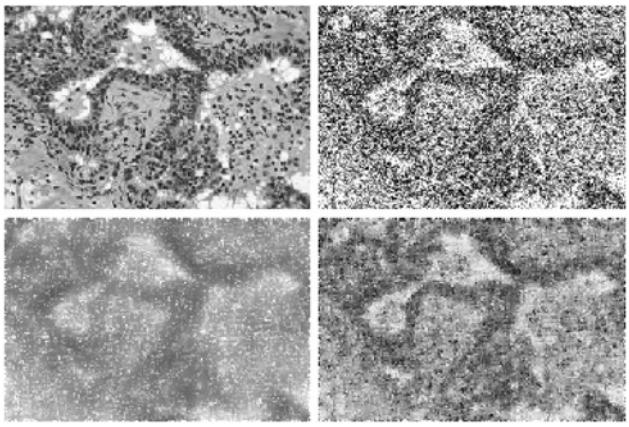

Fig. 2 *Top left-hand side: original prostate tissue. Top right-hand side: noisy image with S2. Bottom left-hand side: denoised image based on BEMD-NLCDP. Bottom right-hand side: denoised image based on tBEMD-NLCDP*

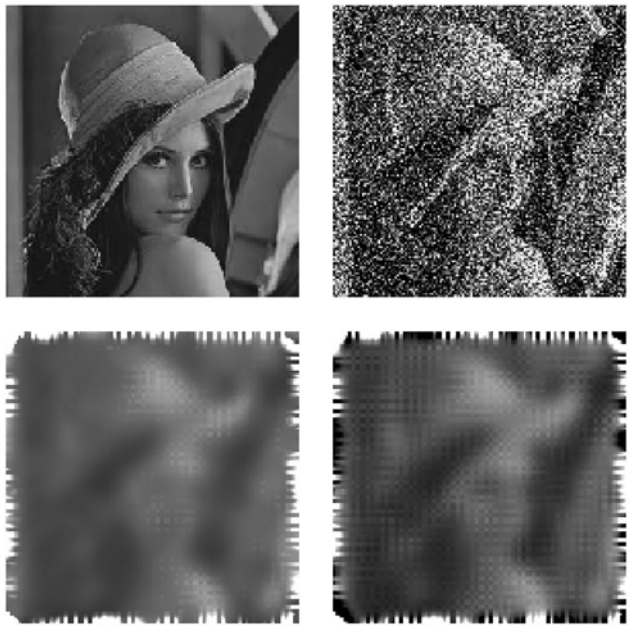

Fig. 3 *Top left-hand side: original Lena image. Top right-hand side: noisy image with S3. Bottom left-hand side: denoised image based on BEMD-LCDP. Bottom right-hand side: denoised image based on tBEMD-LCDP*

(275×183). Each image was converted to greyscale format for processing and Gaussian noise was added to it at varying levels. For instance, the noise had a normal distribution with zero mean and standard deviation $S1 = 0.01$, $S2 = 0.05$, and $S3 = 0.1$. For the DWT thresholding, we considered the Daubechies-4 (db4) and Symlet-4 (sy4) as mother wavelets, and third and fourth levels of decomposition; denoted L3 and L4, respectively. Figs. 1–3 illustrate, respectively, the denoising results of the brain MRI with PDE under $S1$, prostate tissue with NLCDP under $S2$, and Lena image with LCDP under $S3$.

Figs. 4–6 show, respectively, the histogram (with a greyscale colour-bar below) of brain MRI affected with additive noise $S1$, prostate tissue affected with additive noise $S2$, and Lena affected with additive noise $S3$. It is clearly shown that for each noisy image the distribution of pixels is not symmetric and has fat tails. Therefore, the Student's distribution when used to transform data when computing the mean envelope would help capturing heavy tails in the distribution of pixels. In addition, the Student's PDF

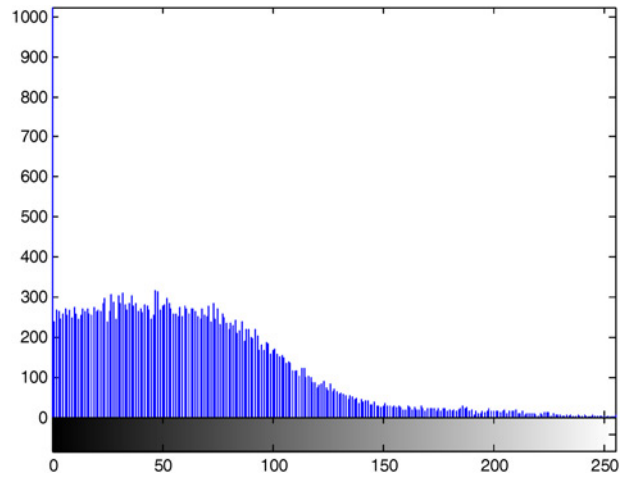

Fig. 4 *Histogram of brain MRI affected with additive noise S1*

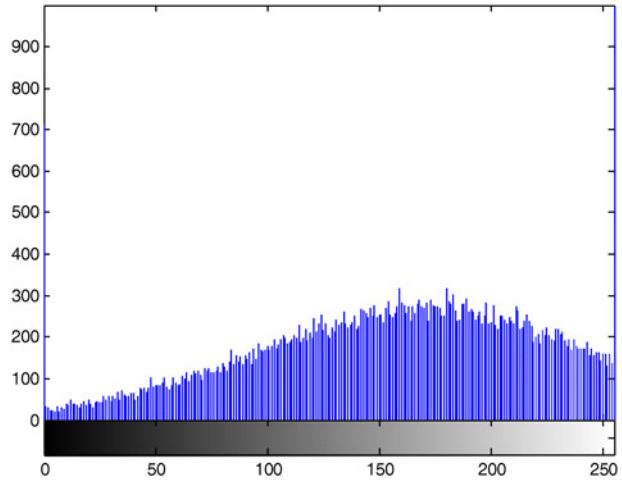

Fig. 5 *Histogram of prostate image affected with additive noise S2*

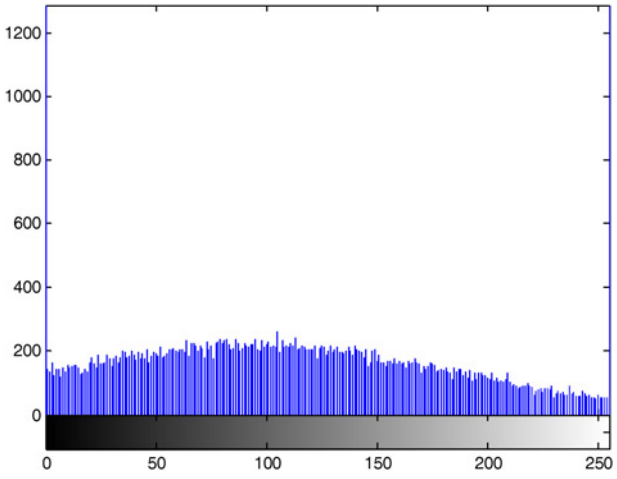

Fig. 6 *Histogram of Lena image affected with additive noise S3*

is prone to capture values that fall far from the mean of the pixels distribution as it has longer tails than the normal distribution.

Table 1 provides the denoising results in terms of PSNR for each type of image. It is well shown that for each level of noise (S), the tBEMD achieved the highest PSNR against the classical BEMD. As a result, BEMD built on Student's distribution probability function (PDF) is more suitable for denoising purpose thanks to its ability to make the original BEMD sifting process robust to values that are far from the mean. Indeed, the robustness of Student's PDF in capturing pixel values far from the mean help improving the estimation of the envelope mean. Finally, on a computer with Intel(R) Core(TM) i5-2500, CPU@3.30 GHz, 4G RAM, and Matlab©2014, the average processing time of the BEMD and tBEMD is, respectively, 9.1510 s and 7.3792 s when noise level is set to *S*1. The average processing time of the BEMD and tBEMD is, respectively, 8.3790 s and 8.4139 s when noise level is set to *S*2. Finally, it is 8.3764 s and 8.4138 for *S*3. Thus, the tBEMD is faster than the classical BEMD when noise level is *S*1 with equivalent processing time when noise level is set to *S*2 or *S*3.

4. Conclusion: We compared the performance of image denoising approaches based the PDE, LCDP, NLCDP, and DWT in BEMD and tBEMD domains. All techniques performed better in tBEMD than in BEMD domain. It is concluded that incorporating the Student's PDF into the sifting process of the classical BEMD helps improving its ability to better denoise images when coupled with PDE, LCDP, NLCDP, and DWT. It is concluded that presented approach is promising for clinical applications.

5. Declaration of interests: None declared.

Table 1 Obtained PSNR for brain MRI, prostate tissue and Lena image

	BEMD (*S*1)	tBEMD (*S*1)	BEMD (*S*2)	tBEMD (*S*2)	BEMD (*S*3)	tBEMD (*S*3)
Brain						
PDE	11.41	**12.24**	10.11	**11.64**	9.02	**10.95**
LCDP	11.68	**12.51**	9.80	**11.15**	8.53	**10.10**
NLCDP	11.39	**12.15**	9.80	**11.33**	8.59	**10.43**
db4-L4	12.19	**12.40**	11.75	**12.04**	11.14	**11.40**
sy4-L4	12.18	**12.40**	11.74	**12.04**	11.15	**11.41**
db4-L3	12.07	**12.15**	11.62	**11.75**	11.03	**11.16**
sy4-L3	12.07	**12.15**	11.62	**11.76**	11.02	**11.15**
Prostate						
PDE	3.30	**3.65**	3.50	**3.78**	3.59	**3.96**
LCDP	3.42	**3.73**	3.51	**3.75**	3.64	**3.99**
NLCDP	3.22	**3.62**	3.26	**3.69**	3.24	**3.80**
db4-L4	3.67	**3.73**	3.84	**3.90**	4.05	**4.10**
sy4-L4	3.66	**3.72**	3.83	**3.89**	4.04	**4.09**
db4-L3	3.66	**3.69**	3.81	**3.84**	4.02	**4.05**
sy4-L3	3.66	**3.68**	3.81	**3.84**	4.02	**4.05**
Lena						
PDE	7.43	**7.82**	6.95	**7.69**	6.52	**7.48**
LCDP	7.41	**7.79**	6.75	**7.41**	6.26	**7.08**
NLCDP	7.41	**7.80**	6.66	**7.53**	6.07	**7.18**
db4-L4	7.85	**7.94**	7.77	**7.88**	7.62	**7.72**
sy4-L4	7.85	**7.93**	7.77	**7.87**	7.63	**7.71**
db4-L3	7.83	**7.86**	7.74	**7.78**	7.58	**7.62**
sy4-L3	7.84	**7.87**	7.74	**7.79**	7.58	**7.62**

Bold values indicates performance of proposed model.

doi: 10.1049/htl.2015.0007

6 References

[1] Huang Z., Shen S.R., Long M.C., *ET AL.*: 'The empirical mode decomposition and the Hilbert spectrum for nonlinear and non-stationary time series analysis', *Proc. R. Soc. London A*, 1998, **454**, pp. 903–995

[2] Lahmiri S., Boukadoum M.: 'Adjusted empirical mode decomposition with improved performance for signal modeling and prediction'. Proc. IEEE LASCAS, 2014, pp. 1–4

[3] Lahmiri S., Boukadoum M.: 'An application of the empirical mode decomposition to brain magnetic resonance images classification'. Proc. IEEE LASCAS, 2013, pp. 1–4

[4] Lahmiri S., Boukadoum M.: 'Automated detection of circinate exudates in retina digital images using empirical mode decomposition and the entropy and uniformity of intrinsic mode functions', *Biomed. Tech./Biomed. Eng.*, 2014, **59**, pp. 357–366

[5] Lahmiri S.: 'A comparative study of ECG signal denoising by wavelet thresholding in empirical and variational mode decomposition domains', *IET Healthc. Technol. Lett.*, 2014, **1**, (3), pp. 104–109

[6] Lahmiri S., Boukadoum M.: 'Pathology grading in retina digital images using Student-adjusted empirical mode decomposition and power law statistics'. Proc. IEEE LASCAS, 2015, pp. 1–4

[7] Pan J.-J., Tang Y.: 'A new image denoising method based on BEMD and self-similar feature'. Proc. IEEE Int. Conf. on Wavelet Analysis and Pattern Recognition (ICWAPR), 2010, pp. 1–5

[8] Yi S., Zeng C.: 'DWI denoising method based on BEMD and adaptive wiener filter'. Proc. IEEE Int. Conf. on Biomedical Engineering and Informatics (BMEI), 2012, pp. 30–34

[9] Liua J., Shi C., Gao M.: 'Image denoising based on BEMD and PDE'. Proc. IEEE Int. Conf. on Computer Research and Development (ICCRD), 2011, pp. 110–112

[10] Xu G.L., Wang X.T., Xu X.G.: 'Improved bi-dimensional empirical mode decomposition based on 2D-assisted signals: analysis and application', *IET Image Process.*, 2011, **5**, pp. 205–221

[11] Donoho D.L., Johnstone I.M.: 'Ideal spatial adaptation by wavelet shrinkage', *Biometrika*, 1994, **81**, pp. 425–455

[12] Donoho D.L.: 'De-noising by soft-thresholding', *IEEE Trans. Inf. Theory*, 1995, **41**, pp. 613–627

[13] Chang S.G., Yu B., Vattereli M.: 'Spatially adaptive wavelet thresholding with context modeling for image denoising', *IEEE Trans. Image Process.*, 2000, **9**, pp. 1522–1530

[14] You Y.-L., Kaveh M.: 'Fourth-order partial differential equations for noise removal', *IEEE Trans. Image Process.*, 2000, **9**, pp. 1723–1730

[15] Gilboa G., Sochen N., Zeevi Y.: 'Image enhancement and denoising by complex diffusion processes', *IEEE Trans. Pattern Anal. Mach. Intell.*, 2004, **26**, pp. 1020–1036